Original Article

Quantitative features of dual-energy spectral computed tomography for solid lung adenocarcinoma with *EGFR* and *KRAS* mutations, and *ALK* rearrangement: a preliminary study

Meng Li[1], Li Zhang[1], Wei Tang[1], Pei-Qing Ma[2], Li-Na Zhou[1], Yu-Jing Jin[1], Lin-Lin Qi[1], Ning Wu[1,3]

[1]Department of Diagnostic Radiology, [2]Department of Pathology, [3]PET-CT Center, National Cancer Center/National Clinical Research Center for Cancer/Cancer Hospital, Chinese Academy of Medical Sciences and Peking Union Medical College, Beijing 100021, China

Contributions: (I) Conception and design: M Li, N Wu; (II) Administrative support: N Wu; (III) Provision of study materials or patients: PQ Ma; (IV) Collection and assembly of data: W Tang, YJ Jin, LL Qi; (V) Data analysis and interpretation: M Li, L Zhang; (VI) Manuscript writing: All authors; (VII) Final approval of manuscript: All authors.

Correspondence to: Ning Wu, MD. Department of Diagnostic Radiology, PET-CT Center, National Cancer Center/National Clinical Research Center for Cancer/Cancer Hospital, Chinese Academy of Medical Sciences and Peking Union Medical College, Beijing 100021, China. Email: cjr.wuning@vip.163.com.

Background: The present work aimed to evaluate radio-genomic associations of quantitative parameters obtained by dual-energy spectral computed tomography (DESCT) for solid lung adenocarcinoma with epidermal growth factor receptor (*EGFR*) and Kirsten rat sarcoma viral oncogene homolog (*KRAS*) mutations, as well as anaplastic lymphoma kinase (*ALK*) rearrangement.

Methods: Ninety-six cases of solid lung cancer were selected and assessed for *EGFR* and *KRAS* mutations, and *ALK* rearrangement. Then, they underwent chest DESCT, and quantitative parameters, including water concentration (WC), iodine concentration (IC), CT value at 70 keV, effective atomic number (Effective-Z) and spectral Hounsfield unit curve slope (λHU slope) were measured. Finally, the associations of quantitative radiological features with various gene alterations were evaluated.

Results: The positive rates were 51.0% (49/96) for *EGFR*, 13.5% (13/96) for *KRAS* and 16.7% (16/96) for *ALK*. In univariate analysis, *EGFR* mutation was associated with smoking status, CT value at 70 keV, IC, Effective-Z, and λHU slope; *KRAS* mutation was associated with CT value at 70 keV, IC, Effective-Z, and λHU slope, and *ALK* rearrangement was correlated with age and WC. In multivariate analysis, smoking status (OR =2.924, P=0.019) and CT value at 70 keV (OR =1.036, P=0.006) were significantly associated with *EGFR* mutation; Effective-Z and age were significantly associated with *KRAS* mutation (OR =0.047, P=0.032) and *ALK* rearrangement (OR =0.933, P=0.008), respectively.

Conclusions: Quantitative analysis of DESCT could help detect solid lung adenocarcinoma harboring *EGFR* or *KRAS* mutation, or *ALK* rearrangement.

Keywords: Dual-energy spectral computed tomography (DESCT); lung adenocarcinoma; *EGFR*; *KRAS*; *ALK*

Submitted Nov 05, 2018. Accepted for publication Aug 15, 2019.
doi: 10.21037/tlcr.2019.08.13
View this article at: http://dx.doi.org/10.21037/tlcr.2019.08.13

Introduction

As the main histological subtype of pulmonary cancer, adenocarcinoma is considered a heterogeneous malignancy based on molecular features (1,2). A recent study demonstrated that patients with lung adenocarcinoma can be treated by novel therapeutics targeting signaling pathways (3). Moreover, precise characterization of lung adenocarcinoma at the genetic level is a fundamental requirement for personalized therapy targeting the involved driver oncogenes.

In general, there are several genetic causes of lung adenocarcinoma, including the most common mutations of the three genes epidermal growth factor receptor (*EGFR*), Kirsten rat sarcoma viral oncogene homolog (*KRAS*) and anaplastic lymphoma kinase (*ALK*). Among these three genes, the *EGFR* oncogene has been widely assessed, therefore becoming a well-established therapeutic target. Studies have shown that tyrosine kinase inhibitors (TKIs) targeting *EGFR* can effectively treat lung carcinoma, improving patient outcome compared with standard platinum-based chemotherapy (4,5). *KRAS*, a Ras GTPase, was first described as a cell growth and division inducer, but is currently considered a non-drug target with insufficient response to standard and targeted therapies (6). *ALK* has attracted considerable attention recently from scientists (7,8). Lung cancer with *ALK* rearrangement is considered a subgroup that shows a striking response to specific targeted drugs, including crizotinib (9,10), which have had approval from the US and Chinese Food and Drug Administrations in 2011 and 2013, respectively (11,12). In the latest guidelines from 2018 by the College of American Pathologists/International Association for the Study of Lung Cancer/Association of Molecular Pathology, the *EGFR* and *ALK* genes must be tested in pulmonary cancer, while *KRAS* is a recommended test gene, especially in cases where routine tests for *EGFR* and *ALK* show negative results (13).

In clinical practice, it is crucial to identify the oncogene status, in order to molecularly categorize lung adenocarcinoma. Computed tomography (CT) is considered the starkest modality for diagnosing lung diseases before surgery. In recent radio-genomics studies, one of the main research aspects has been to explore the relationships between imaging and molecular phenotypes (14). A few studies have explored the possible associations of gene mutations with conventional CT imaging features in order to categorize subclasses of lung adenocarcinoma (15-23). However, conventional CT imaging features are not quantitative, making them vulnerable to the subjectivity of visual judgment. It is now widely recognized that the ground-glass opacity (GGO) ratio is remarkably high in tumors with *EGFR* mutations (15-17), and tumors with *ALK* rearrangement are usually solid nodules (19-22). However, it remains difficult to identify the oncogene status of solid tumors by conventional CT. Meanwhile, identification of the oncogene status is very crucial for patients with solid lung adenocarcinoma, because targeted treatments generally focus on solid tumors in the advanced stage.

In dual-energy spectral CT (DESCT), two consistent energy data sets are generated by the fast-kVp switching technology at 80–140 kVp. Then, monochromatic images are generated from 40 to 140 keV via projection-based reconstruction, which provides quantitative information about different materials (calcium, iodine, water, fat, etc.) based on unique linear attenuation coefficients (24). Therefore, the most prominent advantages of DESCT over conventional CT comprise its set of quantitative analysis tools as well as integrated diagnostic methodology based on multi-parameter images, including material-decomposition images, monochromatic images and spectral curves. DESCT has the potential for characterizing different materials based on elemental composition. Accumulating evidence indicates that DESCT can be employed as a potential diagnostic method in almost all human systems (25-33). With respect to the lung, DESCT has been used for differential diagnosis of tumors from benign lung disease, detecting lymph node metastasis and distinguishing histological subtypes (34), with higher accuracy than conventional CT.

However, studies assessing the associations of DESCT's quantitative parameters with the most commonly encountered genetic mutations in solid lung adenocarcinoma are scarce. Therefore, this work was designed to retrospectively assess DESCT's feasibility for preoperative identification of *EGFR*, *KRAS* and *ALK* status in Chinese cancer cases using the available results for surgically resected solid lung adenocarcinomas.

Methods

The current study was approved by the institutional ethics committee of Cancer Hospital, Chinese Academy of Medical Sciences (No. NCC2016G-029), with waived written informed consent due to anonymous data analysis.

Patient selection

From May 2013 to December 2015, a total of 1,010 patients were retrospectively enrolled from a prospectively collected database of lung nodules and masses. The study group underwent pretreatment chest DESCT at the authors' institution with the following inclusion criteria: presence of solid nodule(s) or mass(es) on CT imaging; histopathological diagnosis of adenocarcinoma. *EGFR* and *KRAS* mutations as well as *ALK* rearrangement were detected after surgery or biopsy at the authors' institution (*Figure 1*).

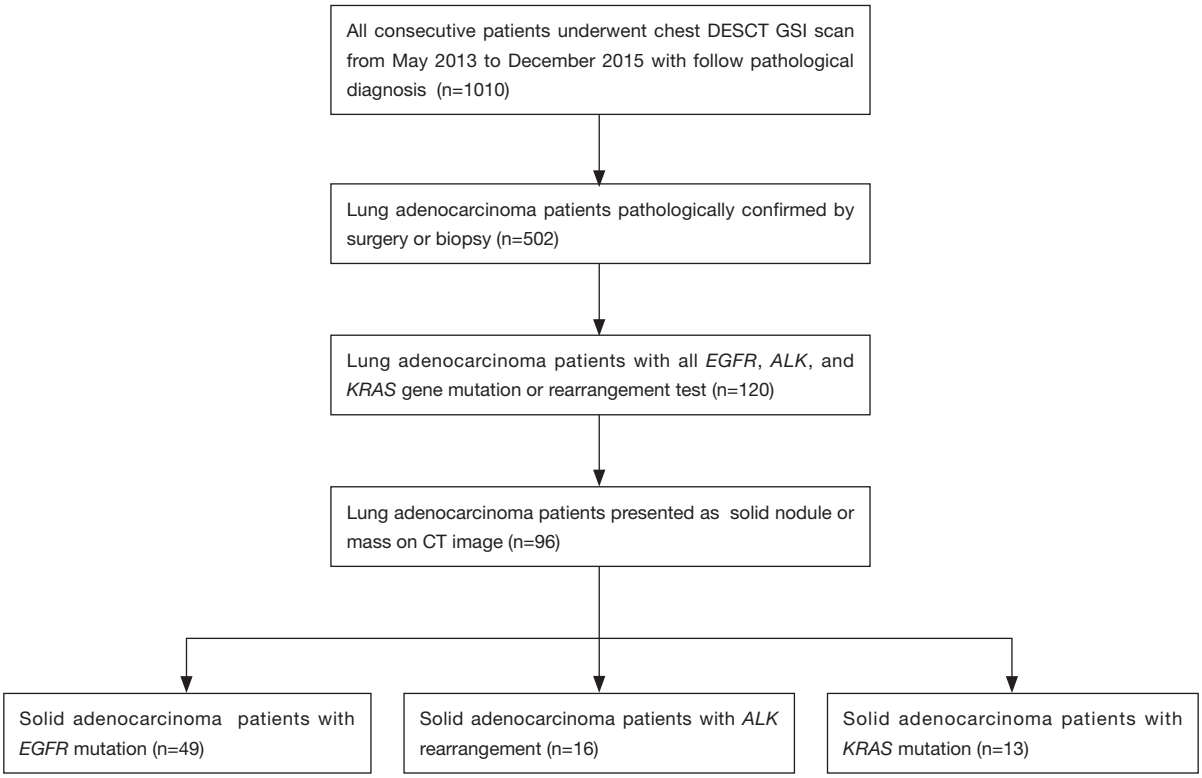

Figure 1 Flowchart depicting the patient selection process. DESCT, dual-energy spectral computed tomography; GSI, gemstone spectral imaging.

DESCT examination

DESCT was carried out on a Discovery CT 750 HD scanner (GE Healthcare, USA) as follows: Gemstone Spectral Imaging (GSI) mode; tube current, 550 mA; rotation time, 0.6 s; pitch value of 0.984 in the helical mode; field of view (FOV), large body; slice interval and thickness for each axial image of 0.8 and 1.25 mm, respectively. Scanning was performed from the lung apex to adrenal glands. Data acquisition was initiated after a delay of 35 s. Cases were intravenously administered 85–100 mL (1.5 mL/kg) of contrast media (Ultravist 300; Bayer Pharma AG) at 2.5 mL/s.

Quantitative analysis of DESCT data

A set of material decomposition (MD) images (iodine/water) and monochromatic images were reconstructed from the original spectral data. Then, GSI Volume Viewer on the post-processing workstation (Advantage Workstation 4.6, GE Healthcare, Milwaukee, WI, USA) was used to analyze the reconstructed images to obtain DESCT's quantitative data.

In order to eliminate the effect of air surrounding the tumors, a mediastinum window (Width =350, Level =50) was used to measure the tumors in axial images. Then, the axial CT slice was selected by an experienced radiologist to depict the maximum diameter of the primary tumor for CT diagnosis of chest tumors. The region of interest (ROI) was selected in the lesion center with a range of less than 2/3 of the total lesion area. The effective atomic number (Effective-Z) of the lesion was recorded from the effective atomic number image. Water concentration (WC) and iodine concentration (IC) were determined from water and iodine-based MD images, respectively. In addition, spectral Hounsfield unit curve slope (λHU slope) was calculated by the following equation: λHU slope = (CT 40 keV – CT 100 keV)/(100–40). Meanwhile, the enhanced CT value in monochromatic images at 70 keV (CT value at 70 keV) was selected since conventional 120 kVp polychromatic images have similar mean energy values as 70 keV GSI images. Therefore, quantitative data included CT value at 70 keV, IC, WC, Effective-Z, and λHU slope.

Analysis of tumor EGFR and KRAS mutations, and ALK rearrangement

The patients' histologic assessment and mutation analyses for the three oncogenes were performed by pathological examinations of surgical (including radical surgery and palliative operation) or biopsy specimens. The mutation status of *EGFR* or *KRAS* was examined by molecular pathological analysis. *ALK* gene rearrangement was detected by immunohistochemistry (IHC).

Statistical analysis

Continuous patient and DESCT variables with normal distribution were expressed as mean ± standard deviation (X ± SD). Normality of variance was assessed by the one-sample Kolmogorov-Smirnov (K-S) test. Associations of patient and DESCT characteristics with gene mutations were assessed by univariate analysis. For normally distributed continuous variables, independent-samples t-test was used. Non-normally distributed continuous variables were analyzed by the non-parametric K-S test. The Chi-square (χ^2) test was employed to assess categorical data. Significant variables in univariate analysis were selected as candidate covariates in subsequent multivariate analysis by the logistic regression model with forward stepwise selection, and odds ratios (ORs) were calculated. The forward stepwise selection process was terminated when a parameter with P=0.05 level could be added to the model with no further effect. Receiver operating characteristic (ROC) curves were used for assessing the predictive values of single or multiple factors for each gene mutation. The area under curve (AUC) was derived to assess the diagnostic value of a given parameter. P<0.05 indicated statistical significance. The SPSS 21.0 statistical software package was used for statistical analysis.

Results

Features of the patients and oncogenes

According to inclusion criteria, 96 patients with solid lung adenocarcinoma (48 men and 48 women averaging 58 years old) submitted to DESCT scanning and *EGFR*, *KRAS* and *ALK* testing after surgery (85 and 7 patients underwent radical and palliative operations, respectively) or biopsy (4 cases) were recruited. The detailed information of the study population is summarized in *Table 1*. There were 49/96 (51.0%), 13/96 (13.5%), 16/96 (16.7%) and 18/96 (18.8%) patients with *EGFR*, *KRAS*, *ALK* and no gene mutations, respectively.

Radio-genomic association of DESCT with EGFR mutation

As shown in *Table 1*, besides smoking status (P=0.004), univariate analysis revealed most DESCT quantitative parameters showed significant associations with EGFR mutation, including CT value at 70 keV, IC, Effective-Z and λHU slope (P=0.001, P=0.038, P=0.037 and P=0.039, respectively). Multivariate analysis demonstrated smoking status (OR =2.924, P=0.019) and CT value at 70 keV (OR =1.036, P=0.006) were both significant factors associated with *EGFR* mutation (*Figure 2*). *Figure 2E* shows *EGFR* mutation prediction based on ROC curves, and the AUC of all factors combined was 0.753.

Radio-genomic association of DESCT with KRAS mutation

As shown in *Table 2*, besides smoking status (P=0.024), univariate analysis revealed cases harboring *KRAS* mutations presented associations with DESCT quantitative parameters, including CT value at 70 keV, IC, Effective-Z and λHU slope (P=0.008, P=0.014, P=0.005 and P=0.014, respectively). Multivariate analysis showed that only Effective-Z (OR =0.047, P=0.032) was significantly correlated with *KRAS* mutations (*Figure 3*). *Figure 3E* shows *KRAS* mutation prediction in ROC curves, and the AUC of the full model was 0.832.

Radio-genomic association of DESCT with ALK rearrangement

Table 3 shows that patients with *ALK* rearrangement had younger age (clinical feature) and lower WC in univariate analysis (*Figure 4*). Multivariate analysis showed that only age (OR =0.933, P=0.008) was significantly associated with *ALK* rearrangement. *Figure 4E* shows *ALK* rearrangement prediction in ROC curves, and the AUC of the full model was 0.748.

Discussion

EGFR, *KRAS* and *ALK* gene alterations were

Table 1 Univariate and multivariate analyses of patient, tumor and DESCT characteristics with *EGFR* mutations

Variables	Total	*EGFR*			Multivariate analysis[+]	
		Mutation	Wild type	P value	OR (95% CI)	P value
No. of patients	96	49	47			
Age (y)		55.6±10.9	55.5±12.6	0.960		
Sex				0.066		
Female	48	29 (59.2)	19 (40.4)			
Male	48	20 (40.8)	28 (59.6)			
Smoking				*0.004*		*0.019*
Smoker	39	13 (26.5)	26 (55.3)		1 (Reference)	
No smoker	57	36 (73.5)	21 (44.7)		2.924 (1.196–7.148)	
Location				0.681		
Central	5	3 (6.1)	2 (4.3)			
Peripheral	91	46 (93.9)	45 (95.7)			
Maximum diameter*	3.3±1.7	3.3±1.4	3.2±1.9	0.420		
DESCT quantitative parameter						
CT value at 70 keV	45.6±20.2	52.2±20.5	38.8±17.6	*0.001*	1.036 (1.010–1.063)	*0.006*
IC	13.9±6.9	15.4±7.3	12.5±6.2	*0.038*		
WC*	1,012.0±17.1	1,015.1±16.0	1,008.8±17.7	0.107		
λHU slope	1.7±0.8	1.8±0.9	1.5±0.7	*0.039*		
Effective-Z	8.4±0.4	8.5±0.4	8.3±0.4	*0.037*		

Numbers in parentheses are percentages. *, non-parametric two-sample K-S test for non-normally distributed continuous data; [+], obtained by a logistic regression model with forward stepwise selection. P<0.05 indicates significant difference; significant P values are in italic. OR, odds ratio; 95% CI, 95% confidence interval; IC, iodine concentration; WC, water concentration; λHU slope, spectral Hounsfield unit curve slope; Effective-Z, effective atomic number.

detected in 51.0% (49/96), 13.5% (13/96), and 16.7% (16/96) patients with solid lung adenocarcinomas, respectively, in the present work. The high *EGFR* mutation rate reflects the genetic characteristic of the East Asian ethnic group, which is completely different from the Western population (4,5,35,36). In contrast, the prevalence of the *KRAS* mutation seems much lower in the East Asian population (37). *KRAS* mutation and *ALK* rearrangement rates in this study were higher than those previously reported (7,38-40). This could be explained by that all patients included in this study had solid adenocarcinomas; indeed, lung adenocarcinomas with *KRAS* mutation and *ALK* rearrangement commonly present as solid nodules with no GGO (20-22). In the present cohort, no patient had two or more gene mutations simultaneously, as these mutations are mutually exclusive.

The current study observed notable associations of *EGFR* mutation with DESCT quantitative indexes, including CT value at 70 keV, IC, Effective-Z and λHU slope in univariate analysis. Meanwhile, only CT value at 70 keV was significantly associated with the above mutation in multivariable analysis. In patients with EGFR mutations, CT values at 70 keV were markedly elevated compared with those of cases harboring wild type *EGFR*. In addition to its role in cancer genesis and development, *EGFR* is involved in both pathological and physiological angiogenetic processes through its effects on both tumor and endothelial cells (41). Furthermore, *EGFR* can upregulate hypoxia-inducible factor α, increasing the expression and secretion levels of angiogenic proteins, including vascular endothelial growth

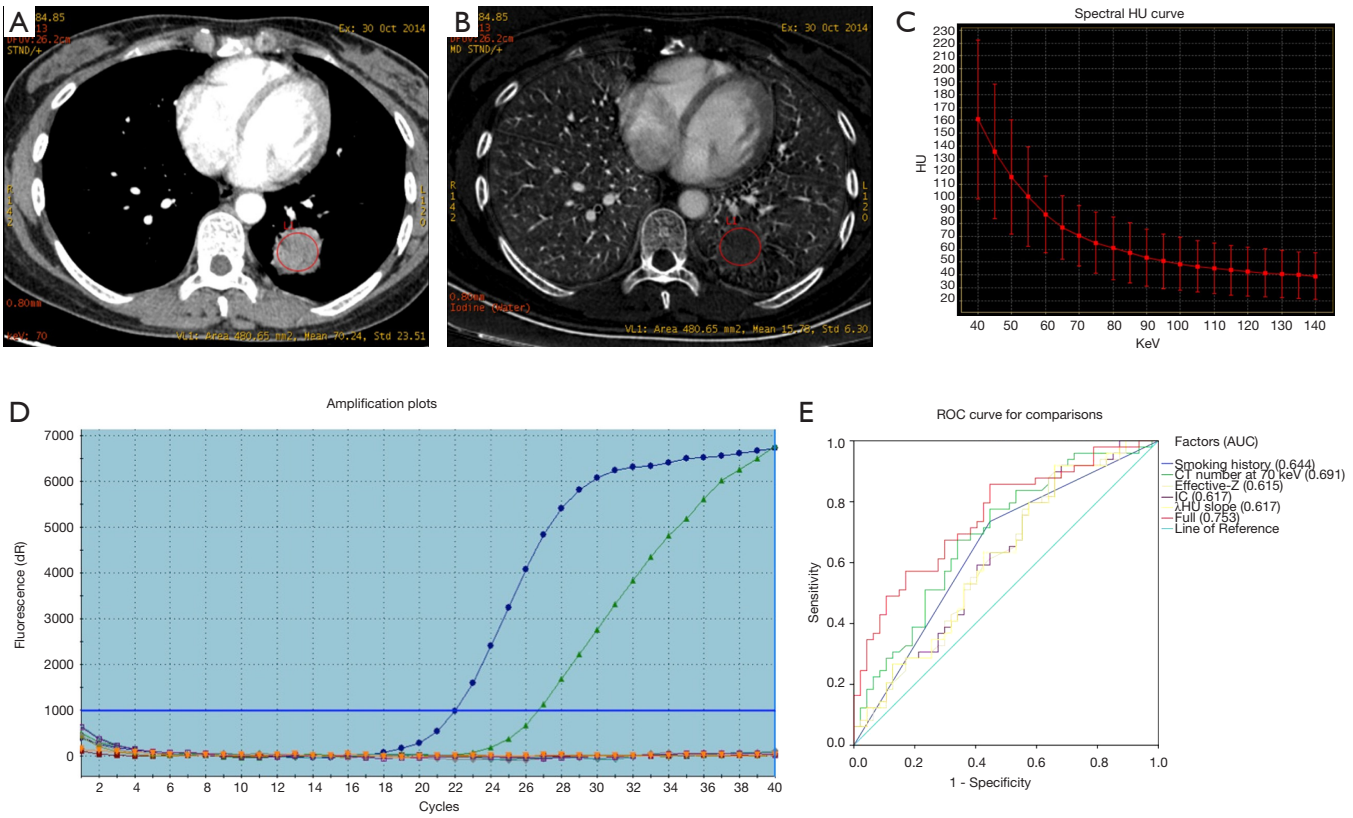

Figure 2 A 44-year-old female diagnosed with *EGFR* mutated lung adenocarcinoma. (A) DESCT 70 keV image showing a solid nodule in the inferior lobe of the left lung, with a CT value at 70 keV of 70.24 HU. (B) Iodine-based material-decomposition image showing an IC of the nodule of 15.78 μg/cm^3. (C) The graph shows the spectral Hounsfield unit curve of the nodule, with a λHU slope of 1.87. (D) Molecular pathological results showing *EGFR* mutations. (E) *EGFR* mutation prediction according to various significant factors and their combination (with AUC =0.753). DESCT, dual-energy spectral computed tomography; IC, iodine concentration; λHU slope, spectral Hounsfield unit curve; ROC, receiver operating characteristic; AUC, area under curve.

factor, thereby stimulating angiogenesis (42). Increased angiogenesis could augment blood supply to the site, which would in turn enhances detection by DESCT. This indicates that DESCT could distinguish different *EGFR* statuses in lung adenocarcinoma. Next, the known association of *EGFR* mutation with the non-smoking status was verified by univariable and multivariable analyses. In this study, women showed an elevated rate of *EGFR* mutations, but the difference was not statistically significant, likely because of the relatively small number of patients assessed. The ROC obtained after combining the significant factors showed a moderate predictive value for *EGFR* mutation identification (AUC =0.753).

KRAS mutations constitute negative prognostic markers in lung adenocarcinoma patients. However, the association of conventional CT imaging with *KRAS* mutation in lung adenocarcinoma is not significant (43). In contrast, *KRAS* mutation and DESCT quantitative parameters, such as CT value at 70 keV, IC, Effective-Z and λHU slope, had significant associations in univariate analysis, as shown above. Meanwhile, only Effective-Z remained significant in multivariate analysis. Lung adenocarcinomas harboring *KRAS* mutations have specific pathological features. In terms of histology, *KRAS* mutations are more associated with mucinous adenocarcinoma or lung cancer showing goblet cell morphology compared with non-mucinous adenocarcinoma (44-46). We speculate that DESCT findings might correlate with the underlying pathologic appearance. The mucus produced by *KRAS* mutant adenocarcinoma may result in a lower quantitative value. As shown above, the ROC obtained by combining all significant factors revealed a moderate predictive value in *EGFR* mutation identification (AUC =0.832).

Table 2 Univariate and multivariate analyses of patient, tumor and DESCT characteristics with *KRAS* mutations

Variables	*KRAS*			Multivariate analysis[+]	
	Mutation	Wild type	P value	OR (95% CI)	P value
No. of patients	13	83			
Age (y)	60.2±8.9	54.9±11.9	0.130		
Sex			0.136		
Female	4 (30.8)	44 (53.0)			
Male	9 (69.2)	39 (47.0)			
Smoking			*0.024*		
Never smoked	4 (30.8)	53 (63.9)			
Smoker	9 (69.2)	30 (36.1)			
Location			0.363		
Central	0 (0.0)	5 (6.0)			
Peripheral	13 (100.0)	78 (94.0)			
Maximum diameter*	3.2±1.3	3.3±1.7	0.923		
DESCT quantitative parameter					
CT value at 70 keV	32.1±21.4	47.8±19.3	*0.008*		
IC	9.7±6.3	14.7±6.8	*0.014*	2.075 (0.939–4.588)	0.071
WC*	1,008.6±18.8	1,012.6±16.9	0.645		
λHU slope	1.1±0.8	1.7±0.8	*0.014*		
Effective-Z	8.1±0.4	8.5±0.4	*0.005*	0.047 (0.005–0.440)	*0.032*

Numbers in parentheses are percentages. *, non-parametric two-sample K-S test for non-normally distributed continuous data. [+], obtained by a logistic regression model with forward stepwise selection. P<0.05 indicates significant difference; significant P values are in italic. OR, odds ratio; 95% CI, 95% confidence interval; IC, iodine concentration; WC, water concentration; λHU slope, spectral Hounsfield unit curve slope; Effective-Z, effective atomic number.

Until recently, fluorescence *in situ* hybridization (FISH) was considered the standard method for *ALK* status testing; however, this technique is not widely applicable due to high cost and long testing time (47,48). Instead, IHC has been intensively used as a screening tool due to easy implementation and affordability for most patients (49). Thus, the latest guidelines state that IHC could replace FISH as the gold standard (13). A recent study indicated that *ALK* positive lung adenocarcinomas testing positive in IHC and negative in FISH might still be successfully treated with crizotinib (50). Therefore, IHC was applied as the gold standard for assessing the *ALK* status in the current study. The above results confirmed that tumors with *ALK* rearrangement had preference for younger age, both by univariate and multivariate analyses. However, in the current study, no DESCT's quantitative parameter of the primary tumor was significantly associated with *ALK* rearrangement in multivariate analyses. WC and CT values at 70 keV were lower in lung adenocarcinoma with *ALK* rearrangement, and WC showed statistical significance (P=0.028). DESCT findings might correlate with the underlying pathologic appearance. Studies showed *ALK* rearrangement mostly occurs in a solid growth pattern with signet-ring cells (51,52). We speculate that WC is reduced in adenocarcinoma with *ALK* rearrangement because less extracellular fluid fills the intercellular space than observed in other subtypes. The ROC obtained by combining all significant factors (including CT value at 70 keV) also showed a moderate predictive value in *EGFR* mutation identification (AUC =0.748).

This study had several limitations. First, the sample size was relatively small, especially the number of cases

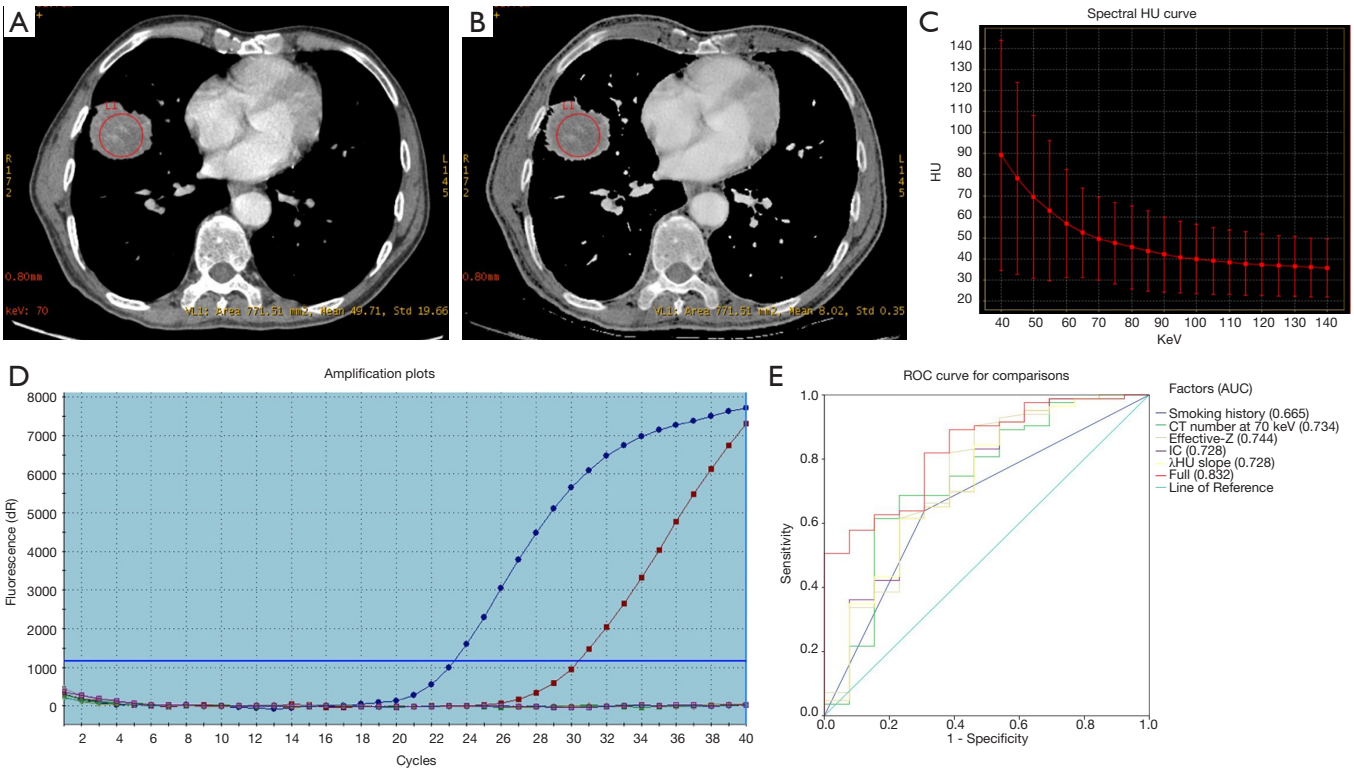

Figure 3 A 67-year-old male diagnosed with *KRAS* mutated lung adenocarcinoma. (A) DESCT 70 keV image showing a solid nodule in the middle lobe of the right lung, with a CT value at 70 keV of 49.71 HU. (B) Effective-Z material-decomposition image showing an Effective Z of the nodule of 8.02. (C) The graph shows the spectral Hounsfield unit curve of the nodule, with a λHU slope of 0.82. (D) Molecular pathological results showing *KRAS* mutations. (E) *KRAS* mutation prediction according to various significant factors and their combination (with AUC =0.832). DESCT, dual-energy spectral computed tomography; Effective-Z, effective atomic number; λHU slope, spectral Hounsfield unit curve; ROC, receiver operating characteristic; AUC, area under curve.

Table 3 Univariate and multivariate analyses of patient, tumor and DESCT characteristics with *ALK* rearrangement

Variables	*ALK*			Multivariate analysis[+]	
	Rearrangement	Wild type	P value	OR (95% CI)	P value
No. of patients	16	80			
Age (y)	48.1±12.7	57.1±10.9	*0.005*	0.933 (0.883–0.982)	*0.008*
Sex			0.584		
Female	7 (43.8)	41 (51.3)			
Male	9 (56.3)	39 (48.8)			
Smoking			0.780		
Never smoked	9 (56.3)	48 (60.0)			
Smoker	7 (43.8)	32 (40.0)			
Location					
Central	1 (6.3)	4 (5.0)	0.837		
Peripheral	15 (93.8)	76 (95.0)			

Table 3 (*continued*)

Table 3 (*continued*)

Variables	*ALK*			Multivariate analysis[+]	
	Rearrangement	Wild type	P value	OR (95% CI)	P value
Maximum diameter*	3.1±2.3	3.3±1.5	0.440		
DESCT quantitative parameter					
CT value at 70 keV	37.4±15.7	47.3±20.6	0.072		
IC	13.6±5.7	14.1±7.2	0.820		
WC*	1,004.8±19.6	1,013.5±16.3	*0.028*	0.972 (0.942–1.003)	0.077
λHU slope	1.6±0.7	1.7±0.9	0.824		
Effective-Z	8.4±0.34	8.4±0.4	0.950		

Numbers in parentheses are percentages. *, non-parametric two-sample K-S test for non-normally distributed continuous data. [+], obtained by a logistic regression model with forward stepwise selection. P<0.05 indicates significant difference; significant P values are in italic. OR, odds ratio; 95% CI, 95% confidence interval; IC, iodine concentration; WC, water concentration; λHU slope, spectral Hounsfield unit curve slope; Effective-Z, effective atomic number.

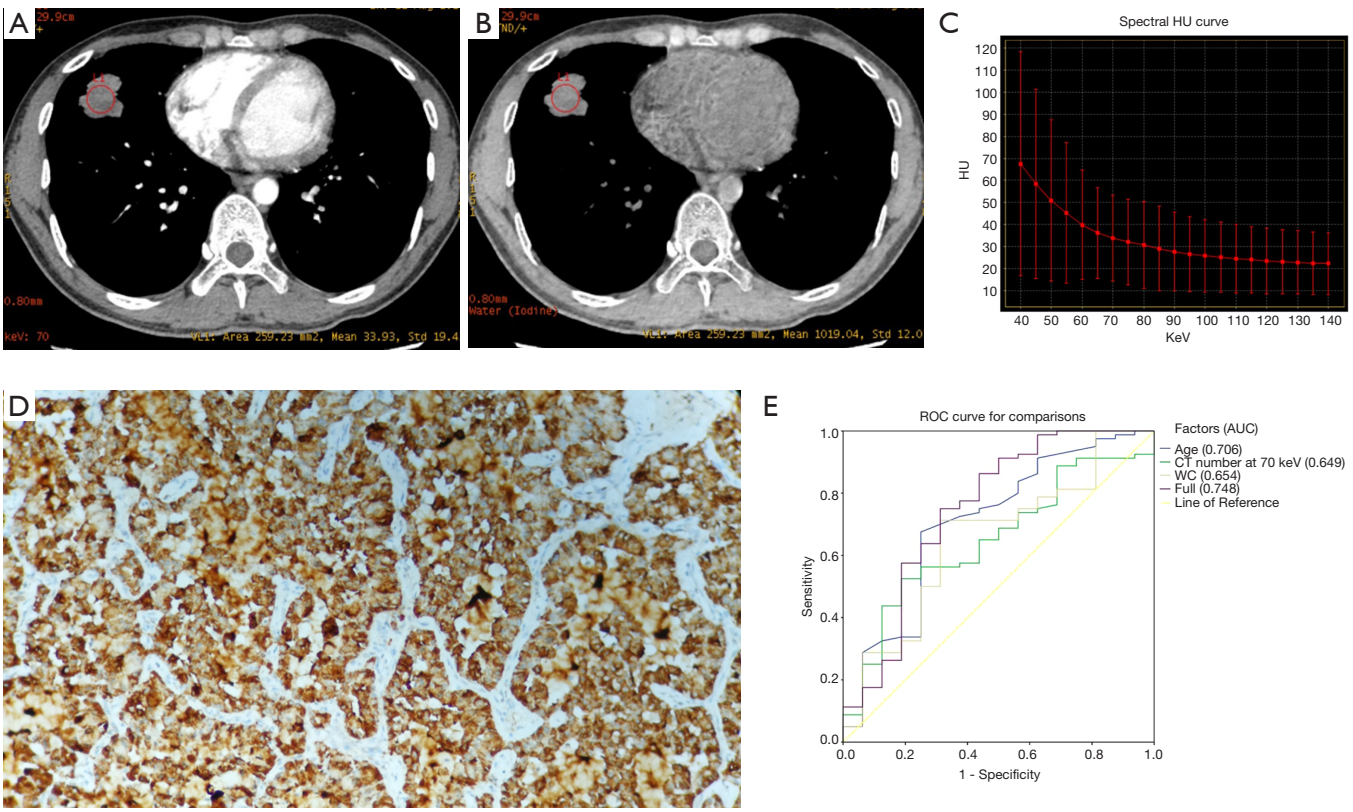

Figure 4 A 28-year-old male diagnosed with *ALK* rearrangement lung adenocarcinoma. (A) DESCT 70 keV image showing a solid nodule in the inferior lobe of the left lung, with a CT value at 70 keV of 33.93 HU. (B) Water-based material-decomposition image showing a WC of the nodule of 1,019.04 μg/cm^3. (C) The graph shows the spectral Hounsfield unit curve of the nodule with a λHU slope of 0.7. (D) Immunohistochemistry showing *ALK* rearrangement. (E) *ALK* rearrangement prediction according to various significant factors and their combination (with AUC =0.748). WC, water concentration; DESCT, dual-energy spectral computed tomography; λHU slope, spectral Hounsfield unit curve; ROC, receiver operating characteristic; AUC, area under curve.

harboring *KRAS* mutations and *ALK* rearrangement. This was due to the low prevalence rates of these mutations. Therefore, the current results must be validated in a larger, multi-institutional cohort. Secondly, most adenocarcinoma patients assessed were candidates for surgical resection, which may result in selection bias toward more pre-advanced cases. Thirdly, many conventional CT features, such as GGO, cavity, bubble-like lucency, and air bronchogram were scarce because all the patients included in this study presented solid lung adenocarcinomas. Moreover, some important non-quantitative conventional CT features, such as spiculation and pleural retraction, were not considered in this study.

Conclusions

Overall, this preliminary radio-genomics study is the first to reveal that quantitative analysis of DESCT has the potential to predict *EGFR* and *KRAS* mutations as well as *ALK* rearrangement in cases with solid lung adenocarcinomas. Compared with other molecular-level technologies, DESCT can provide a comprehensive approach to evaluate the entire tumor non-invasively, which may be incorporated for decision-making in precise diagnosis.

Acknowledgments

The authors wish to thank MedSci for language editorial assistance, Tian Qiu MD for technical assistance in molecular pathology and Jin Guo PhD for providing technical assistance in DESCT.
Funding: This research was supported by the National Natural Science Foundation of China (Grant No. 81601494) and the Fundamental Research Funds for the Central Universities (Grant No. 3332018196). The funding sources were not involved in study design, data interpretation, or article writing.

Footnote

Conflicts of Interest: The authors have no conflicts of interest to declare.

Ethical Statement: The authors are accountable for all aspects of the work in ensuring that questions related to the accuracy or integrity of any part of the work are appropriately investigated and resolved. The study was approved by the institutional ethics committee of Cancer Hospital, Chinese Academy of Medical Sciences (No. NCC2016G-029).

References

1. Travis WD. Reporting lung cancer pathology specimens. Impact of the anticipated 7th Edition TNM classification based on recommendations of the IASLC Staging Committee. Histopathology 2009;54:3-11.
2. Kerr KM. Pulmonary adenocarcinomas: classification and reporting. Histopathology 2009;54:12-27.
3. Buettner R, Wolf J, Thomas RK. Lessons learned from lung cancer genomics: the emerging concept of individualized diagnostics and treatment. J Clin Oncol 2013;31:1858-65.
4. Lynch TJ, Bell DW, Sordella R, et al. Activating mutations in the epidermal growth factor receptor underlying responsiveness of non-small-cell lung cancer to gefitinib. N Engl J Med 2004;350:2129-39.
5. Paez JG, Janne PA, Lee JC, et al. EGFR mutations in lung cancer: correlation with clinical response to gefitinib therapy. Science 2004;304:1497-500.
6. Gerber DE, Gandhi L, Costa DB. Management and future directions in non-small cell lung cancer with known activating mutations. Am Soc Clin Oncol Educ Book 2014:e353-65.
7. Soda M, Choi YL, Enomoto M, et al. Identification of the transforming EML4-ALK fusion gene in non-small-cell lung cancer. Nature 2007;448:561-6.
8. Horn L, Pao W. EML4-ALK: honing in on a new target in non-small-cell lung cancer. J Clin Oncol 2009;27:4232-5.
9. Rodig SJ, Shapiro GI. Crizotinib, a small-molecule dual inhibitor of the c-Met and ALK receptor tyrosine kinases. Curr Opin Investig Drugs 2010;11:1477-90.
10. Casaluce F, Sgambato A, Maione P, et al. ALK inhibitors: a new targeted therapy in the treatment of advanced NSCLC. Target Oncol 2013;8:55-67.
11. Malik SM, Maher VE, Bijwaard KE, et al. U.S. Food and Drug Administration approval: crizotinib for treatment of advanced or metastatic non-small cell lung cancer that is anaplastic lymphoma kinase positive. Clin Cancer Res 2014;20:2029-34.
12. Kazandjian D, Blumenthal GM, Chen HY, et al. FDA approval summary: crizotinib for the treatment of metastatic non-small cell lung cancer with anaplastic lymphoma kinase rearrangements. Oncologist 2014;19:e5-11.

13. Lindeman NI, Cagle PT, Aisner DL, et al. Updated Molecular Testing Guideline for the Selection of Lung Cancer Patients for Treatment With Targeted Tyrosine Kinase Inhibitors: Guideline From the College of American Pathologists, the International Association for the Study of Lung Cancer, and the Association for Molecular Pathology. Arch Pathol Lab Med 2018;142:321-46.
14. Kuo MD, Jamshidi N. Behind the numbers: Decoding molecular phenotypes with radiogenomics--guiding principles and technical considerations. Radiology 2014;270:320-5.
15. Liu Y, Kim J, Qu F, et al. CT Features Associated with Epidermal Growth Factor Receptor Mutation Status in Patients with Lung Adenocarcinoma. Radiology 2016;280:271-80.
16. Lee HJ, Kim YT, Kang CH, et al. Epidermal growth factor receptor mutation in lung adenocarcinomas: relationship with CT characteristics and histologic subtypes. Radiology 2013;268:254-64.
17. Yang Y, Yang Y, Zhou X, et al. EGFR L858R mutation is associated with lung adenocarcinoma patients with dominant ground-glass opacity. Lung Cancer 2015;87:272-7.
18. Yamamoto S, Korn RL, Oklu R, et al. ALK molecular phenotype in non-small cell lung cancer: CT radiogenomic characterization. Radiology 2014;272:568-76.
19. Wang H, Schabath MB, Liu Y, et al. Clinical and CT characteristics of surgically resected lung adenocarcinomas harboring ALK rearrangements or EGFR mutations. Eur J Radiol 2016;85:1934-40.
20. Choi CM, Kim MY, Hwang HJ, et al. Advanced adenocarcinoma of the lung: comparison of CT characteristics of patients with anaplastic lymphoma kinase gene rearrangement and those with epidermal growth factor receptor mutation. Radiology 2015;275:272-9.
21. Halpenny DF, Riely GJ, Hayes S, et al. Are there imaging characteristics associated with lung adenocarcinomas harboring ALK rearrangements? Lung Cancer 2014;86:190-4.
22. Fukui T, Yatabe Y, Kobayashi Y, et al. Clinicoradiologic characteristics of patients with lung adenocarcinoma harboring EML4-ALK fusion oncogene. Lung Cancer 2012;77:319-25.
23. Rizzo S, Petrella F, Buscarino V, et al. CT Radiogenomic Characterization of EGFR, K-RAS, and ALK Mutations in Non-Small Cell Lung Cancer. Eur Radiol 2016;26:32-42.
24. Matsuda I, Akahane M, Sato J, et al. Precision of the measurement of CT numbers: comparison of dual-energy CT spectral imaging with fast kVp switching and conventional CT with phantoms. Jpn J Radiol 2012;30:34-9.
25. Lv P, Lin XZ, Li J, et al. Differentiation of small hepatic hemangioma from small hepatocellular carcinoma: recently introduced spectral CT method. Radiology 2011;259:720-9.
26. Srinivasan A, Parker RA, Manjunathan A, et al. Differentiation of benign and malignant neck pathologies: preliminary experience using spectral computed tomography. J Comput Assist Tomogr 2013;37:666-72.
27. Liu H, Yan F, Pan Z, et al. Evaluation of dual energy spectral CT in differentiating metastatic from non-metastatic lymph nodes in rectal cancer: Initial experience. Eur J Radiol 2015;84:228-34.
28. Hou WS, Wu HW, Yin Y, et al. Differentiation of lung cancers from inflammatory masses with dual-energy spectral CT imaging. Acad Radiol 2015;22:337-44.
29. Li A, Liang H, Li W, et al. Spectral CT imaging of laryngeal and hypopharyngeal squamous cell carcinoma: evaluation of image quality and status of lymph nodes. PLoS One 2013;8:e83492.
30. Liu X, Ouyang D, Li H, et al. Papillary thyroid cancer: dual-energy spectral CT quantitative parameters for preoperative diagnosis of metastasis to the cervical lymph nodes. Radiology 2015;275:167-76.
31. Dong Y, Zheng S, Machida H, et al. Differential diagnosis of osteoblastic metastases from bone islands in patients with lung cancer by single-source dual-energy CT: advantages of spectral CT imaging. Eur J Radiol 2015;84:901-7.
32. Li M, Zheng X, Li J, et al. Dual-energy computed tomography imaging of thyroid nodule specimens: comparison with pathologic findings. Invest Radiol 2012;47:58-64.
33. Graser A, Becker CR, Staehler M, et al. Single-phase dual-energy CT allows for characterization of renal masses as benign or malignant. Invest Radiol 2010;45:399-405.
34. González-Pérez V, Arana E, Barrios M, et al. Differentiation of benign and malignant lung lesions: Dual-Energy Computed Tomography findings. Eur J Radiol 2016;85:1765-72.
35. Haneda H, Sasaki H, Shimizu S, et al. Epidermal growth factor receptor gene mutation defines distinct subsets among small adenocarcinomas of the lung. Lung Cancer 2006;52:47-52.

36. Shigematsu H, Gazdar AF. Somatic mutations of epidermal growth factor receptor signaling pathway in lung cancers. Int J Cancer 2006;118:257-62.
37. Guan JL, Zhong WZ, An SJ, et al. KRAS mutation in patients with lung cancer: a predictor for poor prognosis but not for EGFR-TKIs or chemotherapy. Ann Surg Oncol 2013;20:1381-8.
38. Wong DW, Leung EL, So KK, et al. The EML4-ALK fusion gene is involved in various histologic types of lung cancers from nonsmokers with wild-type EGFR and KRAS. Cancer 2009;115:1723-33.
39. Shaw AT, Yeap BY, Mino-Kenudson M, et al. Clinical features and outcome of patients with non-small-cell lung cancer who harbor EML4-ALK. J Clin Oncol 2009;27:4247-53.
40. Kwak EL, Bang YJ, Camidge DR, et al. Anaplastic lymphoma kinase inhibition in non-small-cell lung cancer. N Engl J Med 2010;363:1693-703.
41. Manning BD, Cantley LC. AKT/PKB signaling: navigating downstream. Cell 2007;129:1261-74.
42. Gordan JD, Simon MC. Hypoxia-inducible factors: central regulators of the tumor phenotype. Curr Opin Genet Dev 2007;17:71-7.
43. Glynn C, Zakowski MF, Ginsberg MS. Are there imaging characteristics associated with epidermal growth factor receptor and KRAS mutations in patients with adenocarcinoma of the lung with bronchioloalveolar features? J Thorac Oncol 2010;5:344-8.
44. Suda K, Tomizawa K, Mitsudomi T. Biological and clinical significance of KRAS mutations in lung cancer: an oncogenic driver that contrasts with EGFR mutation. Cancer Metastasis Rev 2010;29:49-60.
45. Hata A, Katakami N, Fujita S, et al. Frequency of EGFR and KRAS mutations in Japanese patients with lung adenocarcinoma with features of the mucinous subtype of bronchioloalveolar carcinoma. J Thorac Oncol 2010;5:1197-200.
46. Marchetti A, Buttitta F, Pellegrini S, et al. Bronchioloalveolar lung carcinomas: K-ras mutations are constant events in the mucinous subtype. J Pathol 1996;179:254-9.
47. Camidge DR, Hirsch FR, Varella-Garcia M, et al. Finding ALK-positive lung cancer: what are we really looking for? J Thorac Oncol 2011;6:411-3.
48. Atherly AJ, Camidge DR. The cost-effectiveness of screening lung cancer patients for targeted drug sensitivity markers. Br J Cancer 2012;106:1100-6.
49. Conklin CM, Craddock KJ, Have C, et al. Immunohistochemistry is a reliable screening tool for identification of ALK rearrangement in non-small-cell lung carcinoma and is antibody dependent. J Thorac Oncol 2013;8:45-51.
50. Ma D, Wang Z, Yang L, et al. Responses to crizotinib in patients with ALK-positive lung adenocarcinoma who tested immunohistochemistry (IHC)-positive and fluorescence in situ hybridization (FISH)-negative. Oncotarget 2016;7:64410-20.
51. Rodig SJ, Mino-Kenudson M, Dacic S, et al. Unique clinicopathologic features characterize ALK-rearranged lung adenocarcinoma in the western population. Clin Cancer Res 2009;15:5216-23.
52. Yoshida A, Tsuta K, Watanabe S, et al. Frequent ALK rearrangement and TTF-1/p63 co-expression in lung adenocarcinoma with signet-ring cell component. Lung Cancer 2011;72:309-15.

Cite this article as: Li M, Zhang L, Tang W, Ma PQ, Zhou LN, Jin YJ, Qi LL, Wu N. Quantitative features of dual-energy spectral computed tomography for solid lung adenocarcinoma with *EGFR* and *KRAS* mutations, and *ALK* rearrangement: a preliminary study. Transl Lung Cancer Res 2019;8(4):401-412. doi: 10.21037/tlcr.2019.08.13

